Ejecta fragmentation in impacts into gypsum and water ice

K. Miljković, N.J. Mason, J.C. Zarnecki

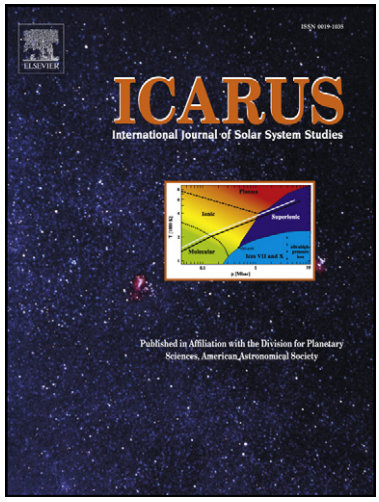

Ejecta fragmentation in impacts into gypsum and water ice

K. Miljković, N.J. Mason, J.C. Zarnecki

PII: S0019-1035(11)00210-7
DOI: 10.1016/j.icarus.2011.05.036
Reference: YICAR 9844

To appear in: *Icarus*

Received Date: 10 February 2010
Revised Date: 29 May 2011
Accepted Date: 31 May 2011

Please cite this article as: Miljković, K., Mason, N.J., Zarnecki, J.C., Ejecta fragmentation in impacts into gypsum and water ice, *Icarus* (2011), doi: 10.1016/j.icarus.2011.05.036

Ejecta fragmentation in impacts into gypsum and water ice

K. Miljković[a,1,*], N. J. Mason[a], J. C. Zarnecki[b]

[a] *Dept. of Physics and Astronomy, The Open University, Walton Hall, MK7 6AA, Milton Keynes, United Kingdom.*
[b] *Planetary and Space Sciences Research Institute, The Open University, Walton Hall, MK7 6AA, Milton Keynes, United Kingdom.*

Abstract

Using the light gas gun at the Open University's hypervelocity impact facility, a series of impact experiments exploring impacts into water ice and gypsum have been performed. Fragmentation of solid ejecta was recorded using two different methods, analysed and compared with the total ejecta. Preliminary results show that the size distribution of the ejecta fragments from water ice is very similar to those from gypsum. These results also represent a step towards a better understanding of ejecta fragmentation in geological materials, including icy surfaces in the Solar system.

Keywords: impact processes, ices, satellites, surfaces.

*Corresponding author
Email address: k.miljkovic@imperial.ac.uk (K. Miljković)
[1]Corresponding address: Imperial College London, Dept. of Earth Sciences and Ingineering, South Kensington Campus, SW7 2AZ, London, United Kindgom

1. Introduction.

Impact induced fragmentation of icy and rocky materials have been studied for half a century. A wide range of data has been acquired for cratering, ejecta fragmentation, ejecta velocity distribution as well as shock induced modification of chemical and physical properties of target materials (e.g. Croft et al. (1979); O'Keefe and Ahrens (1987); Lange and Ahrens (1987); Melosh (1989); Frisch (1992); Iijima et al. (1995); Burchell and Johnson (2005); Hiraoka et al. (2008)). In this study we choose pure water ice and gypsum mineral as target materials. Our work complements previously published experimental fragmentation work. No other experimental work has been reported in measuring the solid ejecta from pure water ice at impact velocities as high as $2\,km\,s^{-1}$. Non-porous policrystaline gypsum ($CaSO_4 \cdot 2H_2O$) was used as a representative of the sulphate class of minerals that hasn't been studied in fragmentation experiments before.

In addition, the aim of this work is to show that pure water ice and non-ice materials (such as gypsum used here) within a family of brittle geological materials fragment in a similar manner and nearly independently of impact conditions during a cratering event. The similar fragmentation between pure ice and gypsum would allow an assumption that a mixture of the two materials would also fragment accordingly. A degree of independence from an impact conditions would allow these results to be applied to planetary scales, but with caution. Since if is difficult to simulate real planetary conditions in the laboratory and study very high velocity impacts, the impacts created in

the laboratory are at smaller scales and speeds. Afterwards, the results are scaled up using different scaling laws.

Ice is widely spread in the Solar system, hence it is important to study it from many aspects. For example, the surfaces of outer moons in the Solar system, such are Europa, Ganymede etc., are mostly covered with water ice. The other surface component is non-icy, usually referred as impurities in ice. The non-ice material on the surfaces of the Galilean satelites is identified as likely to be epsomite ($MgSO_4 \cdot 10H_2O$) (McCord et al., 1998). Epsomite also belongs to a class of sulphate minerals like gypsum. Another example, gypsum was found in northern circumpolar regions of Mars, among other minerals from the same class (Langevin et al., 2005; Wilson and Bish, 2011), indicating that the whole mineral class is represented throughout the Solar system, which is why it is important to start learning their material properties in more details too.

2. Experimental procedure.

2.1. Light gas gun (LGG) assembly and target preparation.

We study the ejecta from impacts made by $1\,mm$ stainless steel ($\rho = 7.86\,g\,cm^{-3}$) balls launched at an impact speed of $2\,km\,s^{-1}$ perpendicularly into either pure water ice or gypsum targets using the LGG in the Hypervelocity Impact (HVI) laboratory at the Open University. The total of 37 impacts into gypsum and 18 into water ice were recorded and analysed.

The LGG assembly at the Open Univesity's Hypervelocity impact labora-

tory is shown in Fig. 1. The high pressure end of the LGG consists of a 0.5" diameter pump tube (27" in length) and a $4.3\,mm$ ($0.17\,cal$) diameter rifled launch tube. The gun is mounted on a tilting frame, which allows horizontal, vertical and oblique incidence operation at impact speeds up to $5\,km\,s^{-1}$, depending on the gas and pressure used (Miljković, 2009; Taylor et al., 2006; McDonnell, 2006). The targets were placed in the small chamber at the end of the gun.

[Fig. 1]

The targets were prepared in-house. Gypsum targets were cut from a larger gypsum block into cubic shapes, $5 \times 5 \times 2.5\,cm$ in size. The gypsum used was polycrystalline with elongated crystals arranged parallel to one another. The porosity was estimated to be $6\,\%$ and $\rho_{bulk} = 2.16\,g\,cm^{-3}$. The water ice targets were $11 \times 11 \times 7\,cm$ in size. They were made using a slow freezing process prepared over $12 - 13\,h$ inside a liquid nitrogen chiller in which the temperature was set to drop at a rate of $11.5^o h^{-1}$. In previous work the cooling rate was reported to be as low as $3^o\,h^{-1}$ (Frisch, 1992), in order to minimise the number of cracks in the ice and prevent any air bubbles from being trapped in the ice target (both of which will significantly alter the fracture profile). However, in our experiments the targets were smaller, so the ramp rate could have been faster. Our final targets were produced crack free, but often with some air bubbles at the bottom of the ice block which weakened the target during the later stages of crater formation only, and did not affect the formation of early and fast ejecta. A cast aluminum 'back plate'

$(11 \times 11 \times 1\,cm)$ was used to support the targets in the impact chamber (Fig. 2). In the case of impacts into ice, the back plate was kept cold by a constant flow of liquid nitrogen through a pipeline drilled in it. The temperature of the ice targets just before impacts was between $175\,K$ and $215\,K$. The target temperature was monitored using tan E-type thermocouples frozen in the water sample near the expected point of projectile impact.

2.2. Ejecta classification and ejecta measurement techniques.

The ejecta resulting from the impact may be separated into two groups, 'early' and 'late'. The early ejecta are composed of small and fast fragments whilst late ejecta are composed of larger fragments that move more slowly. In order to detect both groups, two different detection methods were used. An ejecta profiler for the early, fast ejecta fragments was made of $11\,\mu m$ thin aluminium foil wrapped around $1\,cm$ thick closed-cell plastazote foam. The foam served as a flat support for the Al foil, but it also allowed the capture of ejecta fragments that passed through the foil. It is shaped as a hollow square box with open bases (inner dimensions of $5 \times 5 \times 13\,cm$), as shown in Fig. 2.

[**Fig. 2**]

The early, fast fragments are mostly ejected into a cone, impacting the surrounding foil. Figs. 5 and 6 are examples of impacted foils, showing only one of four sides of the ejecta profiler. However, using this technique, the ejecta moving at angles higher than 80^o (measured from the horizontal) can-

not be recorded, as the top side is opet to allow the projectile to reach the target.

For profiling the later, larger and slower moving ejecta fragments, an additional chamber was placed within the small LGG chamber to collect the ejecta from the target mounted in its bottom. This cylindrical chamber was made from $3\,mm$ thick Al sheet. It had a round base $14.5\,cm$ in diameter and was $30\,cm$ in length. The Al chamber had a hole in the middle of the front lid, $4\,cm$ in diameter to allow the projectile to enter and hit the target. After the shot, the chamber was removed and the ejected fragments collected for analysis. These larger fragments could only be captured in impacts into gypsum, as for the case of ice ejecta, the fragments melt upon contact with the Al chamber wall. However, it should be noted that due to the $4\,cm$ hole on top of the chamber any fragments ejected at angles higher than 85^o could have escaped from the Al chamber.

3. Results.

3.1. Crater morphology and total ejecta mass in gypsum and water ice.

The total ejecta mass in gypsum was measured by the difference in mass before and after filling the impact craters with Apiezon A oil ($\rho = 0.76\,g\,cm^{-3}$). In 8 shots into gypsum, the average total ejecta mass was $0.21 \pm 0.13\,g$. The individual crater dimensions (diameter and depth) and ejecta mass in gypsum are shown in Table 1.

[**Table 1**]

An example of a gypsum crater is shown in Fig. 3 and a vertical profile on Fig. 4. It has also been noticed that the central crater pit was deep, which was due to the crystalline structure of gypsum, where the crystals were long and thin arranged so that the impact happened along crystal's longer side, so the compression wave could travel further along the crystals.

[Fig. 3, Fig. 4]

In all ice impacts the target broke during the cratering event (due to being too small) preventing full crater formation and therefore an accurate measurement of the crater dimensions was not possible, nor could the effects of polycrystalline structure of ice on cratering have been observed. However, we could approximately measure the spall diameter from the largest broken fragments to be $6\,cm$. Using experimentally derived dependences from the earlier ice impact work by Burchell and Johnson (2005), which was performed under similar experimental conditions to ours, the expected ejecta volume, icy ejecta mass, crater diameter and depth in such impact conditions were approximated to $3\,cm^3$, $2.8\,g$, $4\,cm$ and $6\,cm$, respectively.

3.2. Vaporization of gypsum and water ice ejecta.

In order to vaporize, the pressure in the ejecta material needs to be above either incipient threshold (where the solid phase has turned into a mix of liquid and gas) or complete vaporization threshold (the solid has turned into a completely gaseous state) (Zel'dovich and Raizer, 1966). Peak impact pressures occurred in impacts, P_{peak}, were derived from the impedance match

solution using the impact velocity and known equations of state for the projectile and targets materials (Table 2). For gypsum P_{peak} was $23 - 26\,GPa$ and for water ice P_{peak} was $9\,GPa$. Badjukov et al. (1995) reported that gypsum loaded to $56\,GPa$ turns into anhydrite. It is indicative that the shock vaporization of water ice occurs at pressures higher that P_{peak} reached in the experiments, according to e.g. Ahrens and O'Keefe (1984); Stewart and Ahrens (2003) and Stewart et al. (2008). Therefore, it can be concluded that in these experiments any vaporization or significant degassing was not likely to happen.

[**Table 2**]

4. Data analysis.

4.1. Spatial distribution of solid ejecta fragments in gypsum and water ice.

The small and fast fragments were always ejected in a cone shaped distribution, as recorded in the Al foils (Fig. 5 and 6). In our impacts, the ejecta cone in both gypsum and water ice was mostly concentrated around 60^o from the horizontal. This is in agreement with earlier measurements (e.g. Onose (2007); Koschny and Grün (2001) and Evans et al. (1994)). The larger and slower fragments are usually ejected in a nearly vertical direction (e.g. Onose (2007); Koschny and Grün (2001); Polanskey and Ahrens (1990)), hence those fragments were less likely to hit the Al foil, but they also may be too slow to make an imprint in the foil. Unlike gypsum, the spatial distribution of ejected fragments from ice could not be fully determined due

to the weak imprint and low fragment impact count on the foils. In addition to ejecta spatial distribution, in impacts into CO_2 ice, Burchell et al. (1998) reported that about 50 % of the total ejecta were ejected at angles higher than 80^o from the horizontal and that the other half of the ejecta peaked at angles of $60^o - 65^o$, whereas in ice experiments by Frisch (1992), between 50 % and 95 % of the total ejecta mass was ejected at angles $> 80^o$ and no ejecta was found at $< 15^o$ angles. This may also be the reason why there was a low hole and crater count recorded in the foils since such ice fragments have either been ejected at near vertical direction or were melted/vaporized upon contact with the foil.

[Fig. 5, Fig. 6]

4.2. Size distribution of small and fast ejecta fragments in gypsum and water ice.

In gypsum impacts most of the ejected fragments punctured a hole in the foil, from which the size distribution of the ejecta in gypsum could be derived. The impacted foils were placed on a light table and photographed using a 10 Mpx Canon 400D camera with Canon EF 50mm f/1.8 II lens at ISO 800, using 1/50 s exposure. These photographs were then reduced to a grey scale and the conversion from pixel to mm indicated a resolution of $0.04 - 0.06\, mm\, px^{-1}$. A simplified pattern recognition script was written in IDL in order to analyse the images. The script counts the number of holes, represented by white spots on a grey background, then fits the largest possi-

ble circle inside each of the holes and records their radii.

The range of hole sizes in the foils measured in the experiment was $0.05 - 0.3\,mm$. The foil thickness was considerably smaller than the the average hole size, so we could use the equation for near marginal penetration (Eq. 1), that was derived experimentally by Carey et al. (1985). Eq. 1 calculates the fragment diameter, d_p, from measured hole size, D_h, as a function of the fragment speed υ, the thickness of the Al foil ($f = 11\mu m$), the projectile (gypsum) density ($\rho_p = 2.16\,g\,cm^{-3}$), the target (foil) density ($\rho_t = 2.78\,g\,cm^{-3}$).

$$\frac{D_h}{D_p} = 1 + 2.9(\frac{\rho_t}{\rho_p})^{0.6}\frac{f}{d_p}\upsilon^{0.3}\frac{1}{1 + 2.9\frac{\rho_t}{\rho_p}(\frac{f}{d_p})^2\upsilon^{-n}} \tag{1}$$

where $n = 1.02 - 4exp(-0.9\upsilon^{0.9}) - 0.003(20 - \upsilon)$ for $2\,km\,s^{-1} < \upsilon < 20\,km\,s^{-1}$ and $n = 1.02$, $\upsilon > 20\,km\,s^{-1}$.

Since the fragment's impact velocity into the foil is unknown, we use Eq. 2 to substitute for the velocity distribution in Eq. 1. Eq. 2 derived experimentally by McDonnell and Sullivan (1992) calculates the velocity (for a specific foil thickness) a fragments needs to have in order to puncture a hole in the foil. Eq. 2 shows a dependence of the velocity υ of the impactor on the foil (impactee) thickness, f, impactor and target density and strength, ρ_p, ρ_t, σ_{Al}, σ_t, respectively. Conveniently, in our impact experiments $\sigma_{Al} = \sigma_t$.

$$\frac{f}{d_p} = 0.970(d_p)^{0.056}(\frac{\rho_p}{\rho_t})^{0.476}(\frac{\sigma_{Al}}{\sigma_t})^{0.134}\upsilon^{0.701} \tag{2}$$

However, a disadvantage in using a foil for catching the ejecta fragments is that for a fragment of a given mass to make a hole in the foil its impact speed needs to be above the 'ballistic' limit (for that foil thickness), and therefore the foil behaves as a filter. Eq. 2 can only give the minimum speed gypsum fragments had. As already discussed above, the ejecta fragments from water ice probably didn't reach the ballistic limit and therefore only left craters (dimpoles) in the foil. Only a few holes being observed and therefore in the case of water ice the size ejecta distribution was derived from the crater size distribution in the foils. The script could not recognize the crater-like features in the foils since they were of the same light intensity as the rest of the foil. All the foils were therefore also analysed manually (from the photographs) by labelling every crater diameter and converting the pixels into mm, subsequently dividing them into size bins (0.125, 0.375, 0.625 and $0.875\,mm$). For impacts into gypsum (at 90^o incident angle), the number of craters was roughly the same as the number of holes or even higher. According to Kearsley et al. (2008), the diameter of the craters in the Al foil made by ice ejecta fragments corresponds to 3.5 times the ice ejecta size.

In any impact study, the fragmentation can usually be characterized by a power-law function, $N = Ad^{-B}$, where N is the cumulative number of fragments that are larger than a certain size, d. The power-law fits (slope, B and coefficient, A) are shown in Table 3 for gypsum and Table 4 for ice impacts. Holes in the foils made by gypsum ejecta fragments were analysed by the pattern recognition script and double checked visually from the images,

whereas crater-like features in the foils made by ice ejecta were analysed only manually.

[**Table 3, Table 4**]

Cumulative mass distributions of the early ejecta from all shots into ice are shown in Fig. 7. Fig. 8 shows the analysis of small gypsum fragments. Both Figs. 7 and 8 show the sizes of the mass bins that the fragments were distributed in. Bin sizes are large due to the large uncertainty in reading the crater sizes from imaged foils.

[**Fig. 7, Fig. 8**]

4.3. Size distribution of larger gypsum ejecta fragments.

The larger fragments produced from gypsum mostly could not be recorded by the foils. They were either too slow to puncture a hole in the foil or were ejected in a near vertical direction, so the foil could not record them. Therefore, additional impact experiments were conducted in order to profile the larger (spall) fragments using the aluminium chamber (collector) described in Section 2.2. After each shot, the impact ejected fragments confined within the Al chamber were collected from the bottom of the chamber and photographed on a light table. Cumulative ejecta fragment size distributions were determined manually by measuring and counting fragments directly from images. The fragments size range was up to $3\,mm$ starting from the resolution limit at about $0.1\,mm$. These fragments were not spherical, but usually elongated and thin. For imaging, the fragments were placed on the

light table with the largest side facing the camera, effectively hiding the smallest dimension and over sizing the fragments. The measured size distribution was also fitted with a power-law function ($N = Ad^{-B}$) as in the case of the small ejecta fragments. The power-law coefficients and slopes for each shot are shown in Table 5 and the size distributions are shown in Fig. 9. The difference between their slopes is about 10 %, which indicated there is a small variation in slopes between individual impacts. On the other hand, the number of ejected fragments varied significantly which is represented directly in the value of coefficient A.

[**Table 5**]

[**Fig. 9**]

5. Discussion on the ejecta fragmentation.

5.1. The total solid ejecta mass in gypsum and water ice.

The total mass of the small solid ejecta that passed through the foils was calculated assuming all profiled fragments were spherical. The total of larger ejecta mass was recovered from the Al chamber. By comparing the mass of the larger fragments with the total mass ejected from the craters, based on crater volumes, it was calculated that such ejecta fragments comprise some 50 % of the total ejecta mass, whereas the small fragments contribute only a small part of the total ejecta. An interpolation toward the smallest gypsum fragments was made. However, they do not comprise a significant part of the total ejecta mass (as shown in Table 6).

[**Table 6**]

No larger ejecta were measured in water ice. However, larger ejecta fragments in ice are expected to form and to follow the slope of the cumulative size distribution calculated for small ejecta fragments. Their mass was therefore interpolated by extending the size distribution towards the larger fragments (shown in Table 7).

[**Table 7**]

5.2. Complete size distribution of gypsum ejecta fragments.

Mass distributions of both early and late fragments in gypsum were derived from 6 different shots; 3 were performed in order to measure the small fragments and another 3 for measuring the larger fragments. The two distributions, shown in Fig. 10 (and in pale grey in Fig. 11), represent the averaged cumulative size distributions of small and larger fragments and should be overlapping as they represent the ejected fragments from the same target material created in the same impact conditions. However, they do not overlap, and hence corrections were applied for the following reasons (labelled 1 to 5 in Fig. 10): (1) An important consideration in the IDL script used in analysis of the holes in the foils was that the IDL script was programmed to fit the largest possible circle in the hole and record the circle's diameter as the hole size. However, most of the larger holes were elliptical and that means that the larger fragment sizes were undersized. Smaller holes were circular, so the assumption was correct for smaller fragments; (2) Very small

fragments with insufficient mass for creating a hole were proven to exist (via crater like features), and hence the number of the ejected fragments should be increased to correct for such undetected smaller fragments; (3) In the measurement of the larger fragments using the Al chamber, the smaller fragments (in the form of a fine dust) could be lost by sticking to the chamber wall. This means that the number of smaller fragments in the larger fragment population should have been higher; (4) Loss of fragments by ejection in a direction very close to the vertical could have caused a decrease in the number of both smaller and larger fragment distributions, but more likely in the latter, as larger fragments are more likely to move in the near vertical direction. This manifested by not having larger fragments profiled by the foils. (5) Fragments are irregular in shape. A common characteristic among the larger fragments is that they are very thin. Since they are approximated as spheres, it means their mass will be slightly overestimated.

It is not possible to estimate accurately how big the corrections for each of those terms should be. The correction curves that can be approximately quantified are (2), (4) and (5). The number of crater-like features was roughly the same as the number of holes in impacts into gypsum, and therefore this correction can be applied by doubling the number of smaller fragments. The fragments lost due to their moving vertically upwards make no more than 20 % of the total ejecta mass in the case of gypsum. From catastrophic fragmentation research Spina and Paolicchi (1996); Capaccioni et al. (1984) it was found that the shape of the impact created fragments is irregular, but

there is a general correlation between the fragments' dimensions - the ratio between fragment's axes was found to be $2 : \sqrt{2} : 1$. Even though cratering is not a catastrophic event, this ratio was applied to the larger ejecta fragments created in our impact experiments. Assuming that in the images the largest side of the fragment was measured the actual fragment's mass was slightly reduced compared to the spherical assumption. However, in the case of smaller fragments, it should be assumed they spin faster than larger fragments while in motion. In high velocity impacts into basalt, (Fujiwara, 1987) reported that 1 % of the translational kinetic energy of the ejected fragment is spent on the kinetic energy of rotational motion, which is sufficiently high to induce spinning of small fragments on their path from the ejection point and the catcher foil. Therefore, small fragments can pass through the foil at a random orientation during fast spinning, so no size correction need to be made. After applying the size irregularity correction for the larger fragments, the small and large fragment mass distributions overlapped better. Fig. 11 shows (1) to (5) corrections. Fig. 12 also shows the cumulative size distribution for small and larger fragments after corrections for effects (2), (4) and (5).

[Fig. 10, Fig. 11]

It should be noted that by "adding" the larger fragment distribution, the power-law curve fits the distribution better, by flattening the broken part of the distribution for the small fragments at $0.2 - 0.3\,mm$. The new (corrected) linear fit value for the slope is $B = 1.43 \pm 0.17$. This slope

represents an average of all individual impacts analysed in gypsum.

5.3. Comparison between gypsum and ice results.

Fig. 12 shows (i) the size distributions of small and larger gypsum ejecta fragments for all individual shots, derived using the IDL script and (ii) both small and larger fragments determined by a manual count. On the same plot, (iii) the size distributions of the small solid ejecta fragments from ice, from all individual shots, are shown to allow comparison between gypsum and water ice ejecta fragmentation. The cumulative distribution of ice fragments was slightly lower than the cumulative distribution of gypsum fragments. That could be due to possibility that a high percentage of ejected material moves in near vertical direction (Frisch, 1992), but also if the larger fragments move at low speed they might not be able to leave an imprint in the foils, or they are vaporized upon contact with the foil. It is also possible that the motion of some ejecta material excavated at later stages of crater evolution is affected by the ice target breaking up.

[Fig. 12]

These cumulative fragment size distributions in gypsum and ice were re-fitted (after corrections) and new mean slopes obtained of 1.43 ± 0.17 and 1.51 ± 0.25, respectively, which suggests that they fracture in a similar way. Although, the larger ejecta fragments from impacts into ice haven't been recovered, but by comparing the distribution of the measures smaller fragments between ice and gypsum, it is indicative that ice fragments similarly to

gypsum. However, more work is needed to confirm this initial result. Since it is very difficult to conduct impact experiments and measurements on water ice, it is important to find an alternative material that exhibits similar properties to ice and one that is much easier to handle in the laboratory. Table 8 summarizes how gypsum ejecta were partitioned during an impact process. It includes small and larger solid ejecta fragments. Table 9 contains the same information but from impacts into water ice, recorded under the same impact conditions as for gypsum.

[**Table 8, Table 9**]

It should be noted that the total can be smaller than 100 % because: (i) the foils did not cover all possible ejecta angles; and/or (ii) there was a threshold on both ejecta velocity (ballistic limit) and size (imaging resolution), so fragments below the resolution threshold could not be seen. In gypsum, the amount of small fragments is presented as a minimum value because it was expected that some of the ejected fragments were not measured by the foils, whereas the larger fragments collected in the chamber were considered to have been nearly completely collected. The amount of vaporized material in both gypsum and ice was found to be negligibly small.

5.4. Comparison with previous work.

The cumulative size distributions of fragments derived in the impact experiments into gypsum and water ice may be compared with previous work performed using similar geological materials. The compared data was cre-

ated under different experimental (impact) conditions (projectile speed, size and incidence angle) and measured using different techniques in different fragment size ranges, as shown in Table 10. Our slopes of the fragmentation distribution, B, are comparable to the values reported by other authors, but it is the most similar to the fragmentation in other experiments in ices and ice-silica mixtures. In the case of CO_2 ice, Burchell et al. (1998) derived two distributions or one that showed 'a knee' which they fitted with two slope values. In this work, the distribution of small fragments showed a similar property, a break in the slope that was afterwards corrected by adding the larger fragments (Fig. 12). The temperatures of ice targets were different in experiments performed by other groups and this indicates that the fragmentation of the ejected material in an impact event also does not depend significantly on the target temperature.

The ejecta fragmentation (via the slope of the cumulative size distribution of the ejected fragments) in a cratering event in a geological material seems not to strongly depend on the impact incident angle, the projectile speed or the projectile material and shape, even when the fragmentation has been observed and analysed using different techniques, such as the Deep Impact event (Jorda et al., 2007). Jorda et al. (2007) acquired the ejecta fragmentation result from the data gathered by the OSIRIS narrow angle camera onboard Rosetta spacecraft during an encounter with the comet 9P/Tempel-1.

[**Table 10**]

6. Conclusions.

Our results provide new data for high velocity impact fragmentation of gypsum and pure ice in a cratering event. The comparison with other authors for similar (brittle, geological) materials at a range of impact conditions indicated that the fragmentation seems not to be strongly dependent on impact parameters such are projectile material, size, speed, or incident angle. Apart from the traditional fragmentation studies, these results could be further applied to a study of impact ejecta fragmentation on a planetary body, assuming that the investigated geological materials are adequate analogues for icy planetary surfaces and re-scaling laws properly implemented, since impact events in the Solar system are usually at higher speeds than investigated in this study. Higher impact energies induce higher pressures and temperatures in the target material, therefore a significant amount of melt and vapour could be expected next to a portion of material ejected as fragmented solid. The total ejecta volume seems to be roughly scalable with impact energy (Burchell et al., 2001). Then, using shock physics laws, material equations of state and its shock response properties, the portion of the material ejected as solid could be modelled. For that portion, the fragmentation law and results obtained in this study could be applied, to get an estimate of the number of ejected fragments into the surrounding space.

References

Ahrens, T. J., Johnson, M. L., 1995. A Handbook of Physical Constants. 2. AGU, Ch. Shock wave data for minerals, pp. 143–184, AGU Reference Shelf.

Ahrens, T. J., O'Keefe, J. D., 1984. Shock vaporization and the accretion of the icy satellites of jupiter and saturn. LPSC XV, 3–4.

Badjukov, D. D., Dikov, Y., Petrova, T. L., Pershin, S. V., 1995. Shock behavior of calcite, anhydrite, and gypsum. LPSC XXVI (26), 63–64.

Burchell, M. J., Brooke-Thomas, W., Leliwa-Kopystynski, J., Zarnecki, J. C., 1998. Hypervelocity impacts on solid CO2 targets. Icarus 131, 210–222.

Burchell, M. J., Grey, I. D. S., Shrine, N. R. G., 2001. Laboratory investigations of hypervelocity impact cratering in ice. Adv. Space Res. 28 (10), 1521–1526.

Burchell, M. J., Johnson, E., 2005. Impact craters on small icy bodies such as icy satellites and comet nuclei. Mon. Not. R. Astron. Soc. 360, 769–781.

Capaccioni, F., Cerroni, P., Coradini, M., Farinella, P., Flamini, E., Martelli, G., Paolicchi, P., Smith, P. N., Zappalá, V., 1984. Shapes of asteroids compared with fragments from hypervelocity impact experiments. Nature 308, 832–834.

Carey, W. C., McDonnell, J. A. M., Dixon, D. G., 1985. Capture cells: decoding the impacting particle parameters. LPSC XVI, 111–112.

Croft, S. K., Kieffer, S. W., Ahrens, T. J., 1979. Low-velocity impact craters in ice and ice-saturated sand with implications for martian crater count ages. J. Geophys. Res. 84 (B14), 8023–8032.

Durda, D. D., Flynn, G. J., 1999. Experimental study of the impact disruption of a porous inhomogeneous target. Icarus 142, 46–55.

Evans, N. J., Shahinpoor, M., Ahrens, T. J., 1994. Large Meteorite Impacts and Planetary Evolution. Vol. 293. Geol. Soc. Am., Ch. Hypervelocity impact: ejecta velocity, angle and composition, pp. 92–101.

Frisch, W., 1992. Hypervelocity impact experiments with water ice targets. In: McDonnell, J. (Ed.), Proc. of the workshop Hypervelocity impacts in space. Unit for Space Sciences, University of Kent, Canterbury, pp. 7–14.

Fujiwara, A., 1987. Energy partition into translational and rotational motion of fragments in catastrophic disruption by impact: An experiment and asteroid cases. Icarus 70, 536–545.

Gaffney, E. S., Ahrens, T. J., 1980. Identification of ice vi on the hugoniot of ice ih. Geophys. Res. Lett. 7, 407–409.

Hermalyn, B., Schultz, P. H., Heineck, J. T., 2010. The ejecta evolution of deep impact: Insight from experiments. AGU Fall Meeting Abstract, P53C–1522.

Hiraoka, K., Arakawa, M., Setoh, M., Nakamura, A. M., 2008. Measurements of target compressive and tensile strength for application to impact cratering on ice-silicate mixtures. J. Geophys. Res. 113 (E02013), 7.

Iijima, Y., Kato, M., Arakawa, M., Maeno, N., Fujimura, A., Mizutani, H., 1995. Cratering experiments on ice: Dependence of crater formation on projectile materials and scaling parameters. Geophys. Res. Lett. 22 (15), 2005–2008.

Jorda, L., Lamy, P., Faury, G., Keller, H. U., Hviid, S., Küppers, M., Koschny, D., Lecacheux, J., Gutiérrez, P., Lara, L. M., 2007. Properties of the dust cloud caused by the deep impact event. Icarus 187, 208–219.

Kato, M., Iijima, Y., Arakawa, M., Okimura, Y., Fujimura, A., Maeno, N., Mizutani, H., 1995. Ice-on-ice impact experiments. Icarus 113, 423–441.

Kearsley, A. T., Graham, G. A., Burchell, M. J., Cole, M. J., Wozniakiewicz, P., Teslich, N., Bringa, E., Hörz, F., Blum, J., T., Poppe, 2008. Microcraters in aluminum foils: Implications for dust particles from comet wild 2 on nasa's stardust spacecraft. Int. J. Impact Eng 35 (12), 1616–1624.

Kondo, K.-I., Ahrens, T. J., 1983. Heterogeneous shock-induced thermal radiation in minerals. Phys. Chem. Minerals 9, 173–181.

Koschny, D., Grün, E., 2001. Impacts into icesilicate mixtures: Crater morphologies, volumes, depth-to-diameter ratios, and yield. Icarus 154, 391–401.

Lange, M. A., Ahrens, T. J., 1987. Impact experiments in low-temperature ice. Icarus 69, 506–518.

Langevin, Y., Poulet, F., Bibring, J.-P., Gondet, B., 2005. Sulfates in the north polar region of mars detected by omega/mars express. Science 307 (5715), 1584–1586.

Larson, D. B., Bearson, G. D., Taylor, J. R., 1973. Shock-wave studies of ice and two frozen soils. In: PCwC, T. L., Mackay, J. R. (Eds.), North American Contribution to the Second International Conference on Permafrost. pp. 318–325.

Matuska, D. A., 1984. Hull users manual.

McCord, T. B., Hansen, G. B., Clark, R. N., Martin, P. D., Hibbitts, C. A., Fanale, F. P., Granahan, J. C., Segura, M., Matson, D. L., Johnson, T. V., Carlson, R. W., Smythe, W. D., Danielson, G. E., 1998. Non-water-ice constituents in the surface material of the icy galilean satellites from the galileo near-infrared mapping spectrometer investigation. J. Geophys. Res. E4, 8603–8626.

McDonnell, J. A. M., 2006. The open university planetary impact facility: A compact two-stage light gas gun for all impact angles. Int. J. Impact Engng. 33, 410–418.

McDonnell, J. A. M., Sullivan, K., 1992. Hypervelocity impacts on space detectors; decoding the projectile parameters. In: McDonnell, J. (Ed.),

Proc. of the workshop Hypervelocity impacts in space. Unit for Space Sciences, University of Kent, Canterbury, pp. 39–48.

Melosh, H. J., 1989. Impact cratering. a geological process. Oxford university press, Oxford monographs on geology and geophysics.

Miljković, K., 2009. Investigation of the dust around europa by impact experiments and modelling. Ph.D. thesis, The Open University, UK.

Miljković, K., Mason, N. J., Zarnecki, J. C., 2009. Research on europa's dust cloud at the open university's hvi laboratory. ISTS Special Issue: Selected papers from the 26th International Symposium on Space Technology and Science Tr2 (7), 37–39.

O'Keefe, J. D., Ahrens, T. J., 1987. The size distributions of fragments ejected at a given velocity from impact craters. Int. J. Impact Engng 5, 493–499.

Onose, N., 2007. Mass-velocity distribution of fragments in oblique impact cratering on gypsum: Two groups of fragments and their ejection mechanisms. Ph.D. thesis, ISAS/JAXA, Japan.

Polanskey, C., Ahrens, T. J., 1990. Impact spallation experiments: fracture patterns and spall velocities. Icarus 87 (1), 140–155.

Simakov, G. V., Pavlovskiy, M. N., Kalashnikov, N. G., Trunin, R. F., 1974. Shock compressibility of twelve minerals. Izv. Earth Phys. IO, 488–492.

Spina, A. L., Paolicchi, P., 1996. Catastrophic fragmentation as a stochastic process: sizes and shapes of fragments. Planet. Space Sci. 44 (12), 1563–1578.

Stewart, S. T., Ahrens, T. J., 2003. Shoch hugoniot of H2O ice. Geophys. Res. Lett. 6 (1332).

Stewart, S. T., Seifter, A., Obst, A. W., 2008. Shocked H2O ice: Thermal emission measurements and the criteria for phase changes during impact events. Geophys. Res. Lett. 35 (L23203).

Taylor, E. A., Batham, M. G., Gilmour, M. A., Green, S. F., Hall, C., McBride, N. M., McDonnell, J. A. M., Miljković, K., Towner, M. C., Watson, K. V., Zarnecki, J. C., September 2006. The open university hypervelocity impact laboratory. In: 57th ARA meeting proc. Venice, Italy.

Wilson, S. A., Bish, D. L., 2011. Formation of gypsum and bassanite by solid-state mineral reactions: Implications for the bioavailability of water on mars. LPSC 42nd.

Zel'dovich, Y. B., Raizer, Y. R., 1966. Physics of shock waves and high-temperature hydrodynamic phenomena. Academic Press, Inc., New York, USA.

Zhang, F., Sekine, T., 2007. Impact-shock behaviour of mg- and ca-sulfates and their hydrates. Geochim. et Cosmochim. Ac. 71, 4125–4133.

Tables

Table 1. Crater dimensions for 8 different impact events. D_{spall} is the averaged spall diameter, d_{inner} is the diameter of the central pit, H_{spall} is the depth of the spall (crater terrace), h_{inner} is the central pit depth and m is the total ejecta mass. Crater diameter and depth parameters are labelled in Figs. 3 and 4.

Shot No.	D_{spall} [mm]	D_{inner} [mm]	H_{spall} [mm]	h_{inner} [mm]	m [g]
KM00024	7.00	1.26	1.68	5.59	0.12
KM00037	4.61	1.44	1.14	6.29	0.03
KM00038	6.31	1.03	2.19	6.20	0.17
KM00039	6.48	1.17	2.06	5.57	0.20
KM00040	6.95	0.89	3.20	6.88	0.23
KM00050	10.02	1.04	1.36	6.31	0.47
KM00052	6.81	1.49	0.98	5.99	0.14
KM00055	6.42	1.25	2.46	6.38	0.31

Table 2. Shock equations of state for gypsum and water ice used to calculate peak shock pressures.

Target material	C_o	s	Author
Gypsum	2.8	1.95	Ahrens and Johnson (1995)
	5.2	0.5	Ahrens and Johnson (1995)
	2.49	1.79	Simakov et al. (1974), Kondo and Ahrens (1983), Ahrens and Johnson (1995), Zhang and Sekine (2007)
Water ice	1.43	1.48	Larson et al. (1973), Gaffney and Ahrens (1980), Ahrens and Johnson (1995)
Stainless steel	4.61	1.73	Matuska (1984)

Table 3. Cumulative hole distribution arising from early ejecta in gypsum targets in different impact events. $N_{holes,IDL}$ is the number of holes counted using the IDL script, $N_{crat.,holes}$ is the total number of craters and holes (dimpoles) counted manually in the foils, A is the coefficient and B is the slope of the cumulative fragments' size distribution.

Shot No.	$N_{holes,IDL}$	$N_{crat.,holes}$	a	B
KM00024	1014	5742	40	1.33
KM00039	2113	4740	78	1.20
KM00040	2028	7134	66	1.30

Table 4. Cumulative hole distribution arising from early ejecta in ice targets. $N_{crat.,holes}$ is the total number of craters and holes (dimpoles) counted manually in the foils, A is the coefficient and B is the slope of the cumulative fragments' size distribution.

Shot No.	$N_{crat.,holes}$	A	B
KM00056	531	12	1.50
KM00058	848	10	1.35
KM00062	631	15	1.31
KM00064	1270	62	1.31
KM00066	3539	4	1.60
KM00067	2136	22	1.48
KM00068	2758	27	1.50

Table 5. Parameters of the cumulative size distribution arising from larger fragments in gypsum from 3 different impact experiments made under the same impact conditions. $N_{frag.}$ is the number of larger fragments collected in the Al chamber after an impact, A_{larger} and B_{larger} are the coefficient and the slope of the cumulative size distribution of the collected larger gypsum fragments.

Shot No.	$N_{frag.}$	A_{larger}	B_{larger}
KM00053	1283	9	2.71
KM00055	815	18	2.57
KM00050	1117	54	2.40

Table 6. The ejected mass in the form of early and late ejecta fragments in gypsum. Small fragments ($0.05 < d < 0.4\,mm$) and larger fragments ($0.1 < d < 2.0\,mm$ in size) were measured and interpolation towards even smaller fragments ($d < 0.05\,mm$) was calculated. Some overlap in size range between small and larger fragments can be also seen in Fig. 11.

Shot No.	Small [g]	Small (Interp. [g])	Larger [g]
KM00024	0.008	0.0007	-
KM00039	0.016	0.002	-
KM00040	0.020	0.02	-
KM00050	-	-	0.193
KM00053	-	-	0.109
KM00055	-	-	0.181

Table 7. The ejected mass in the form of early and late ejecta fragments in ice. Small fragments ($d < 0.3\,mm$) were measured via craters (dimpoles) in the foils and the larget fragments ($d > 0.3\,mm$) were extrapolated from the distribution of the small fragments.

Shot No.	Small [g]	Larger (Interp.) [g]
KM00056	0.0002	0.009
KM00058	0.0004	0.007
KM00062	0.0003	0.010
KM00064	0.0005	0.044
KM00066	0.0013	0.003
KM00067	0.0009	0.017
KM00068	0.0012	0.021

Table 8. The partition of the total gypsum ejecta mass according to two different measurements and the expected loss of the ejecta mass.

Type of fragments	% of the total mass
Solid - small fragments that made holes in the foil	$\geqslant 8$
Solid - small fragments that made craters in the foil	$\geqslant 8$
Solid collected large fragments	~ 50
Near vertically ejected fragments; lost fragments	$\leqslant 35$

Table 9. The partition of the total ice ejecta mass according to two different measurements and the expected loss of the ejecta mass.

Type of fragments	% of the total mass
Solid - small fragments that made craters and holes in the foil	$\ll 1$ (from raw data) ~ 0.4 (corrected)
Larger fragments ejected at near vertical direction and/or too slow for foil profiling.	50-95 (Frisch, 1992)
Late ejecta fragments lost in target breaking up.	<50

Table 10. Comparison of the power-law slopes B of ejecta fragmentation in different geological materials. Target stands for target material and Impact conditions stand for projectile material, incidence angle and impact speed, respectively. Impact angle of the projectile is given in *degrees*, impact velocity, v, in $km\,s^{-1}$. Ice temperature in ^oC shown in brackets for ices.

Target	Impact conditions	B	Author
Olivine basalt	Al sphere, 90,5	2.7 ± 0.1	Durda and Flynn (1999)
Compact ice-silicate mixture	Glass/Nylon, 90, $0.9 - 11.4/1.1 - 3.3$	1.6 ± 0.3	Koschny and Grün (2001)
Comet 9P/ Tempel 1	Deep Impact probe, 30, 10	2.1 ± 0.3	Jorda et al. (2007) Hermalyn et al. (2010)
Polycrystalline gypsum	stanless steel, 30/60/90, 2	1.25 ± 0.20	Miljković et al. (2009)
Polycrystalline gypsum	stanless steel, 90, 2	1.43 ± 0.17 for small and 2.47 ± 0.14 for larger ejecta	This work
Water ice (-18)	water ice, $15\,mm$ in diam., $10\,mm$ long, 90, 1	2.4 ± 0.3	Kato et al. (1995)
CO_2 ice (-43)	stainless steel, $0.4 - 2.0\,mm$ in diam., 90, 5	0.75 ± 0.25 for small and 1.5 ± 0.5 for larger ejecta	Burchell et al. (1998)
Water ice $(-97$ to $-7)$	glass, $18 - 124\,\mu m$, 90, 1.8-9.6	1.75 ± 0.26	Frisch (1992)
Water ice (-83 ± 15)	stainless steel, $1\,mm$ in diam., 90, 2	1.51 ± 0.25	This work

Figure captions

Fig. 1. Two stage light gas gun (LGG) assembly at the Hypervelocity Impact (HVI) laboratory at the Open University. Time-of-flight (TOF) unit is composed of two separated laser curtains. When a projectile passed through, the TOF sends a signal, which provides the information about the projectile speed. Primary blast tank stops most of the blast during projectile launch. Launcher is composed of the riffled barrel and the pump tube. Compression of a light gas (He, N_2 or H_2) in the pump tube creates conditions for the acceleration of a projectile.

Fig. 2. The target setup in the small LGG chamber. Al foil wrapped around the foam was placed against the target. Target was supported by the back plate. The back plate was chilled for ice impacts by a flow on liquid nitrogen through it. Projectile entered from the left. The ejecta fragments created upon impact hit the foil and left an imprint (holes and dimpoles) and an example shown in Figs. 5 and 6.

Fig. 3. Impact crater in gypsum (shot KM00024), showing crater inner, d_{inner}, and spall, D_{spall}, diameters (also in Table 1).

Fig. 4. Crater parameters labelled on a cross section of an ideal impact crater in gypsum, D_{spall}, d_{inner}, H_{spall} and h_{inner}.

Fig. 5: One of four sides of a foil used for capturing early ejecta fragments in gypsum. The foil width is $4\,cm$. Projectile hit from the top down causing the ejecta to lift from down up into a conical shape, hence leaving a parabolic imprint in the foils.

Fig. 6: One of four sides of a foil used for capturing early ejecta fragments in ice. The foil setup is the same as in Fig. 5. Imprint in foils caused by ice ejecta was weaker than in the case of gypsum, probably due to weaker and slower ejecta than in case of gypsum.

Fig. 7: Cumulative size distributions of early ejecta fragments from all shots into water ice targets. Holes and dimpoles were chategorised into size bins (0.125, 0.375, 0.625 and 0.875 mm).

Fig. 8: Cumulative size distributions of early ejecta fragments from all shots into gypsum (KM00024, KM00039 and KM00040), measured both by using the IDL script (for holes only) and manually (for both holes and dimpoles).

Fig. 9: Cumulative size distribution of larger ejecta fragments from impact into gypsum collected from the Al chamber (collector).

Fig. 10: Corrections of the raw data applied due to: (1) ellipticity of the larger holes in the foil; (2) existence of dimpoles (craters) in the foil; (3) loss of very small fragments; (4) loss of larger fragments ejected in the near vertical direction; (5) fragments' irregular shape.

Fig. 11: Averaged measured (shown in pale grey) and corrected (shown in black) cumulative size distribution of both small and larger fragments in gypsum impacts. Corrected distribution is made by quantifying and implemening the corrections (1) to (5) from Fig. 10.

Fig. 12: Cumulative size distributions of all measured ejecta fragments from all shots into gypsum and water ice, showing some sim-ilarity in fragmentation between pure water ice and gypsum.

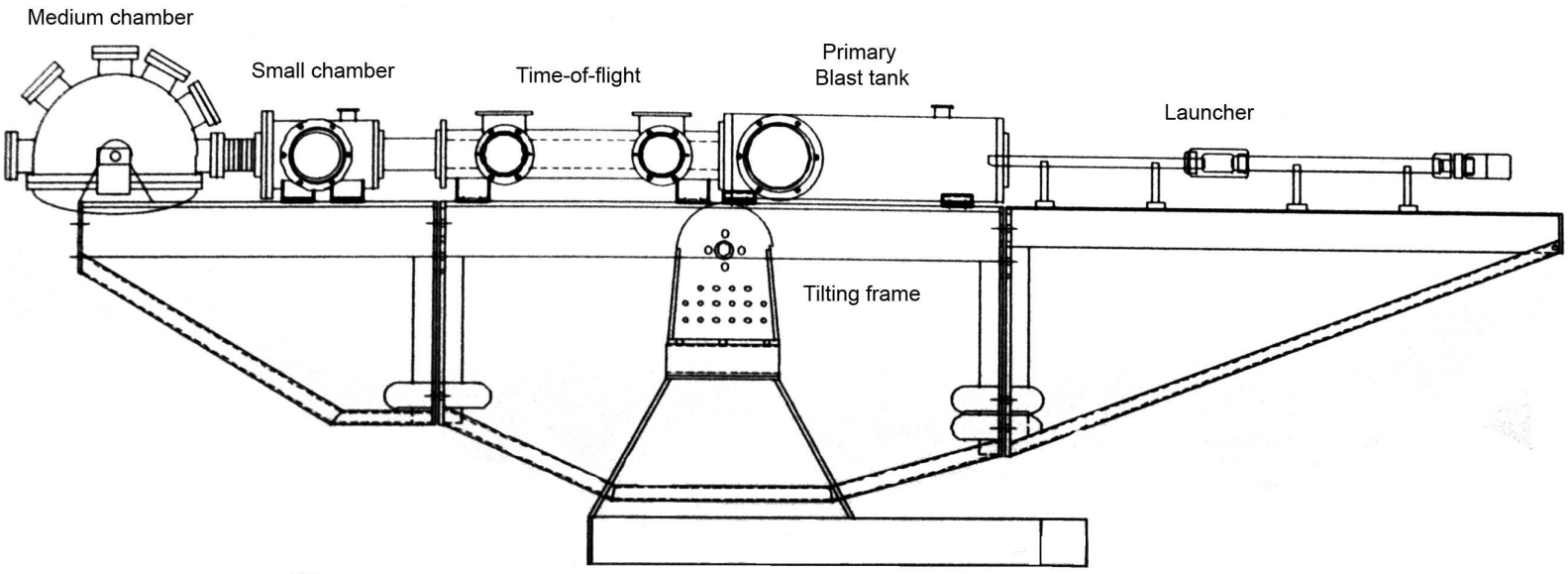

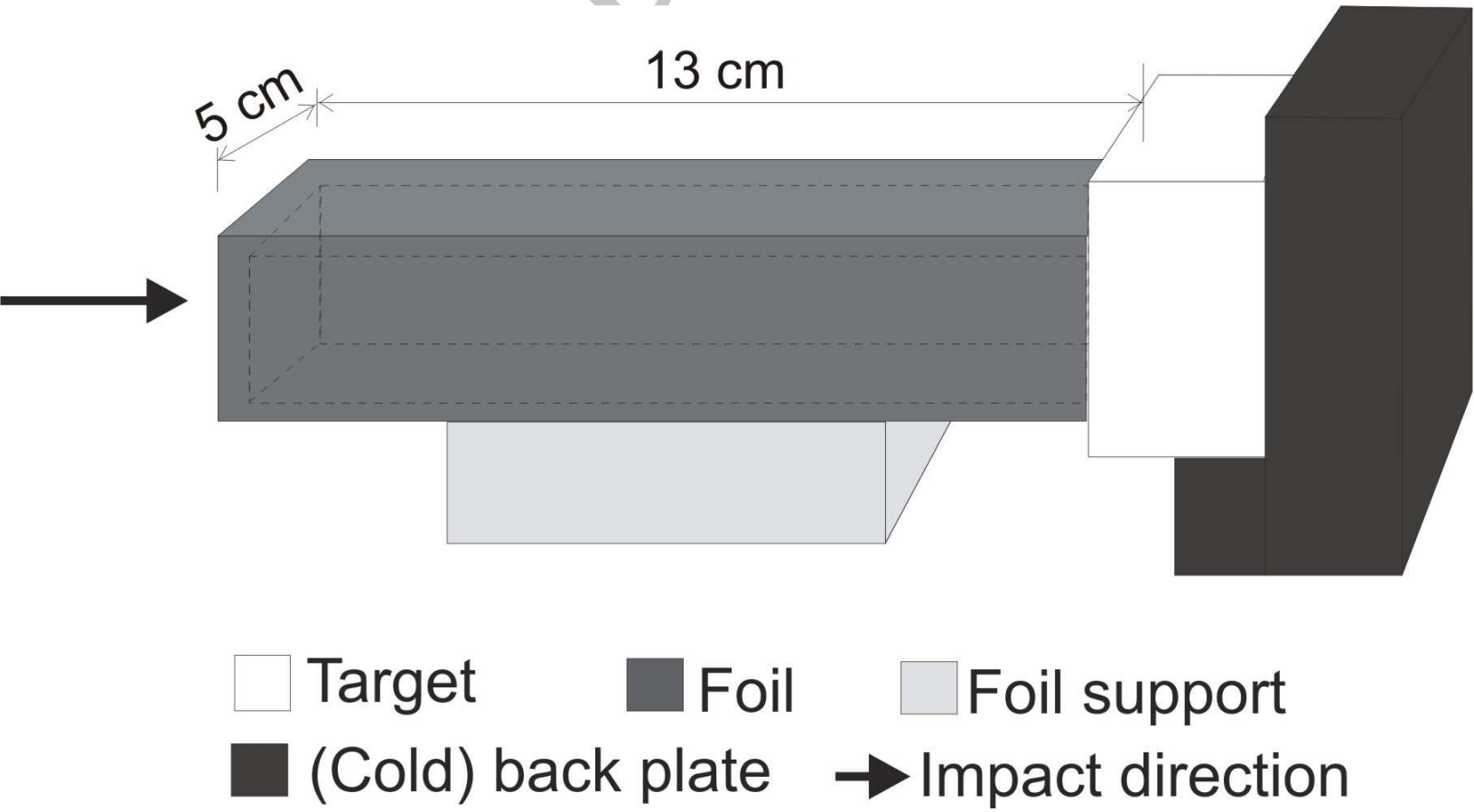

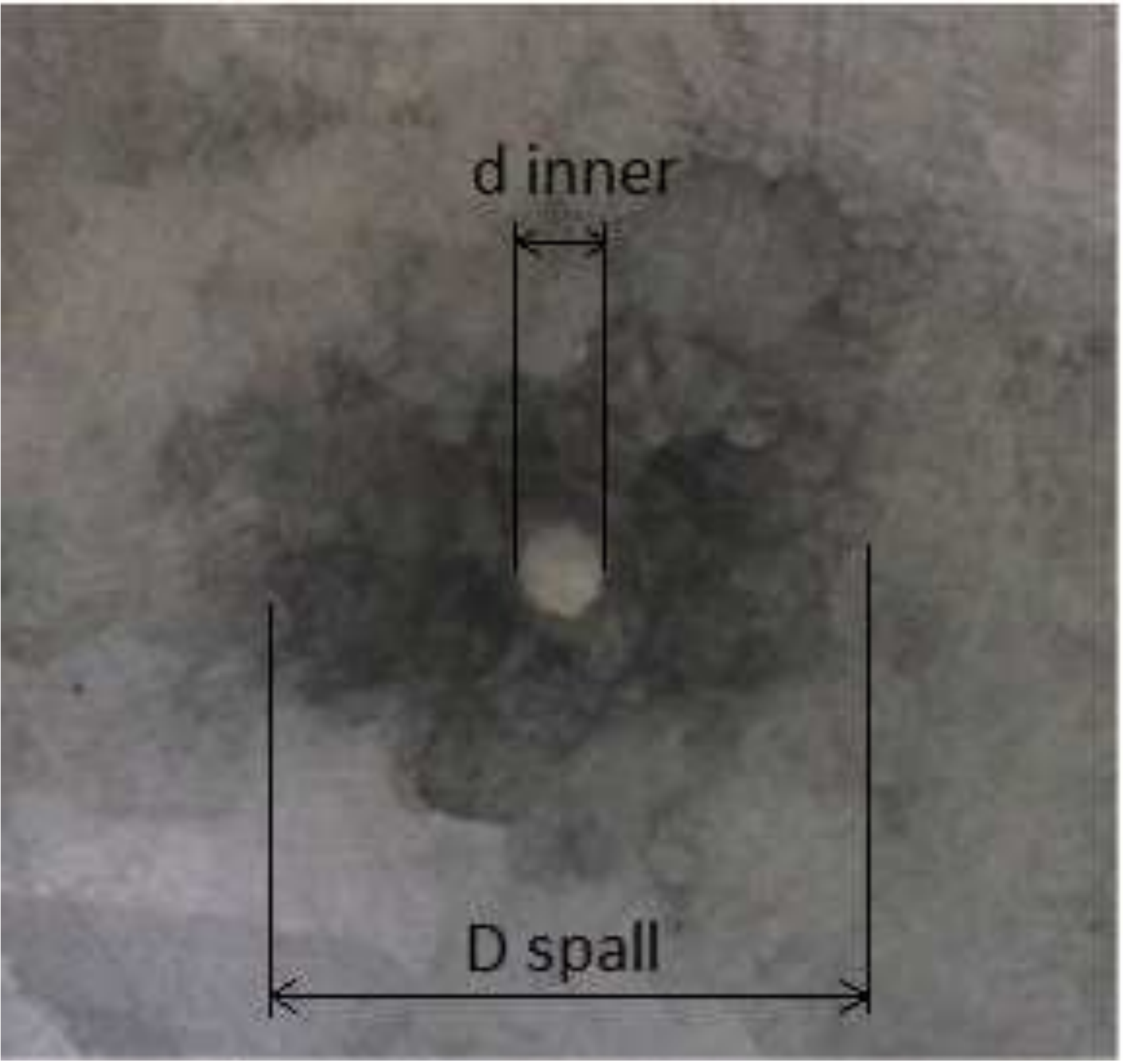

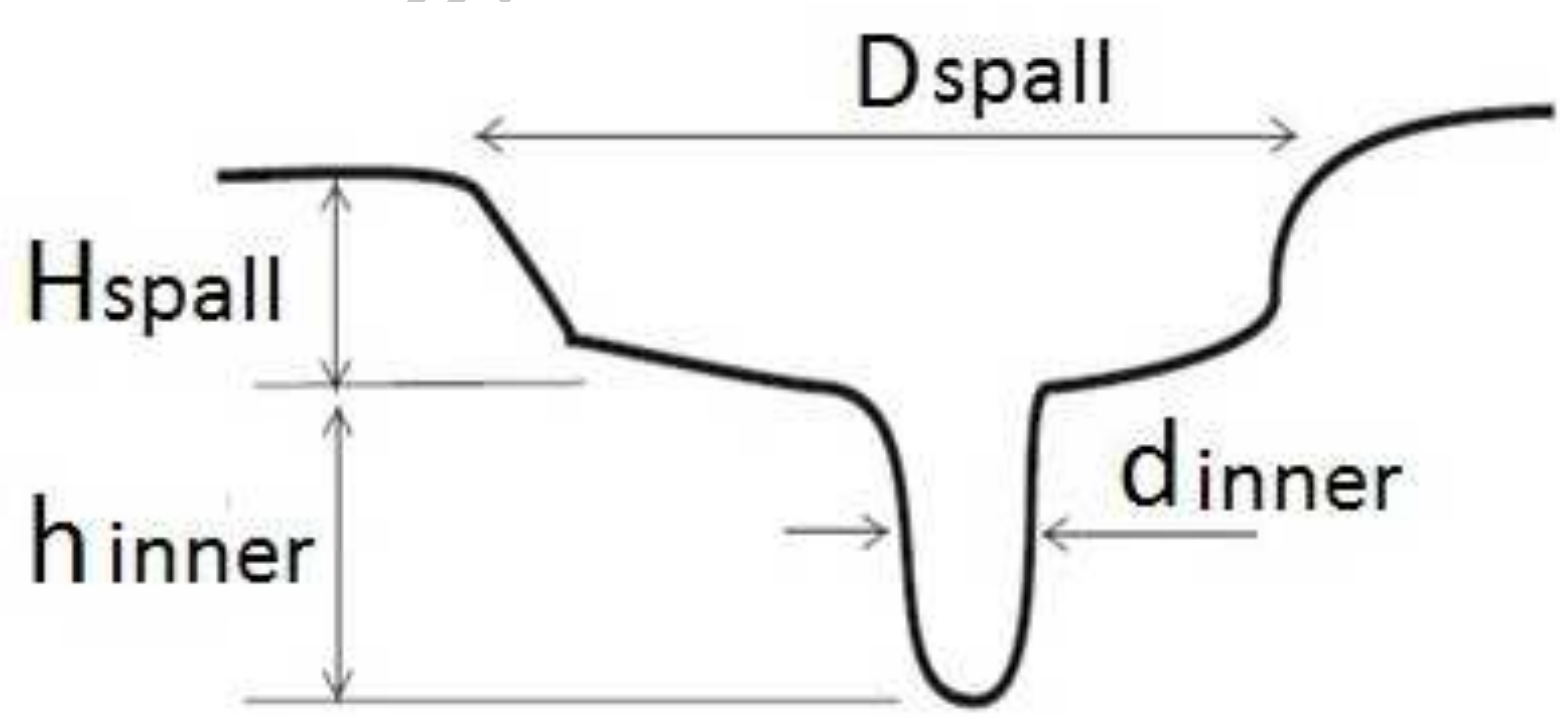

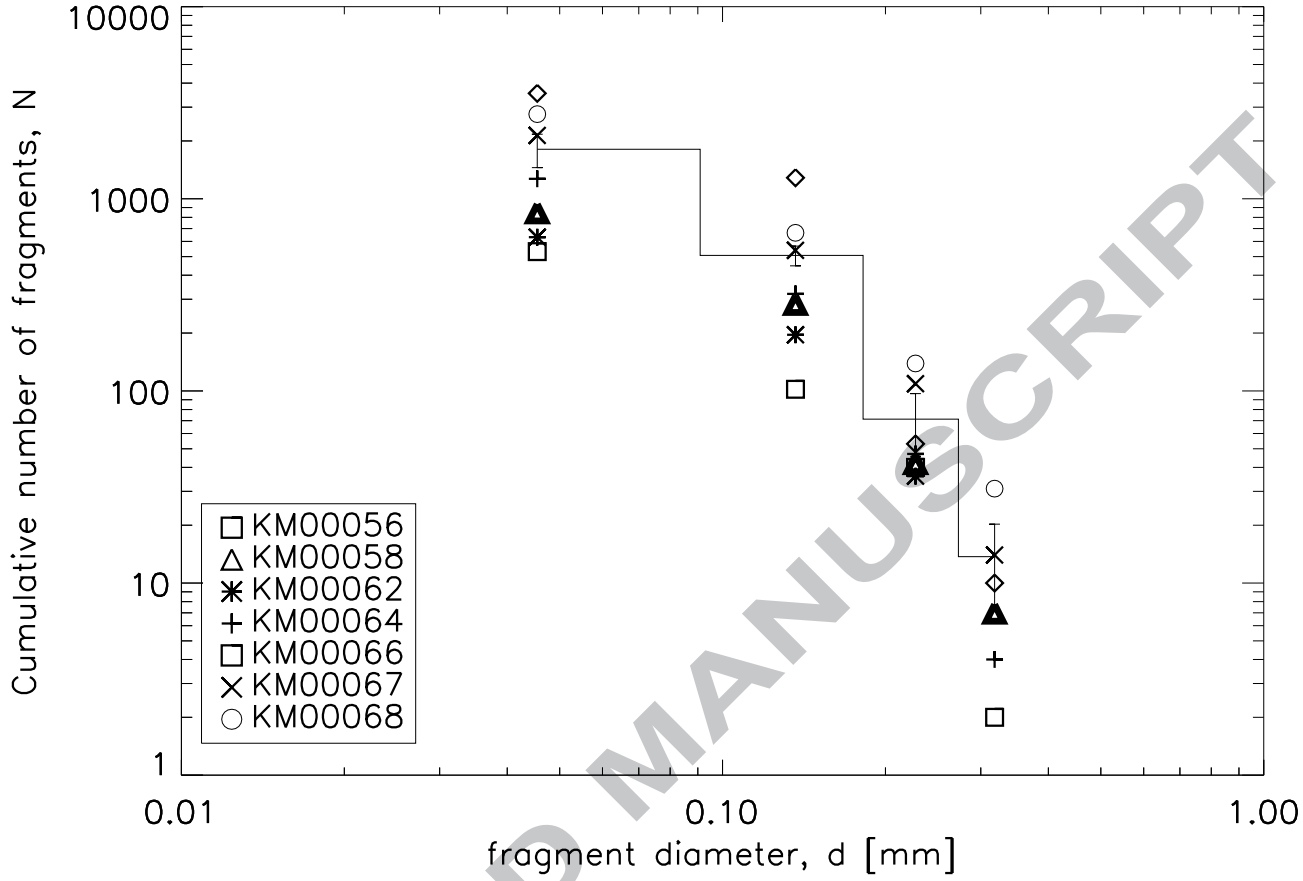

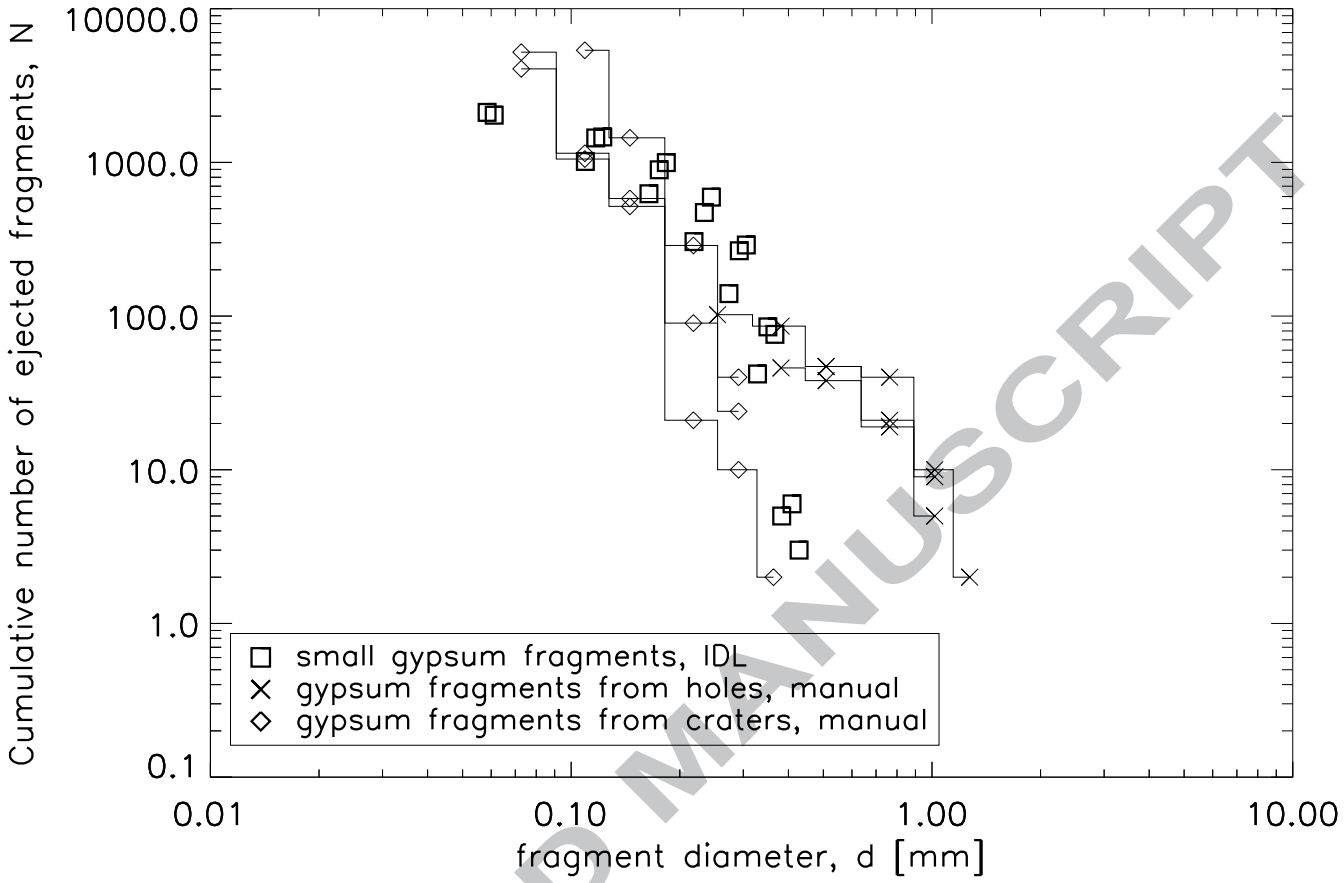

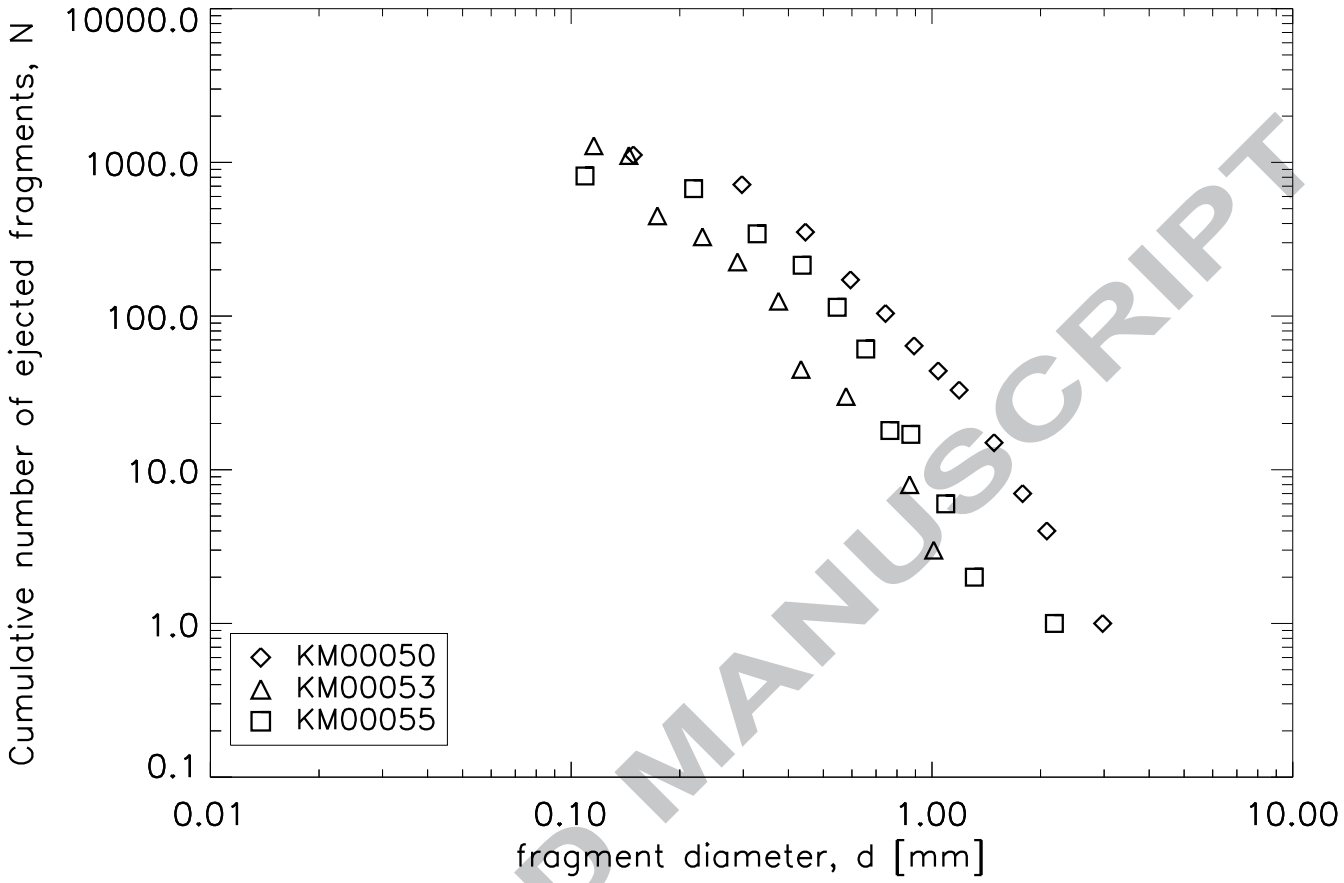

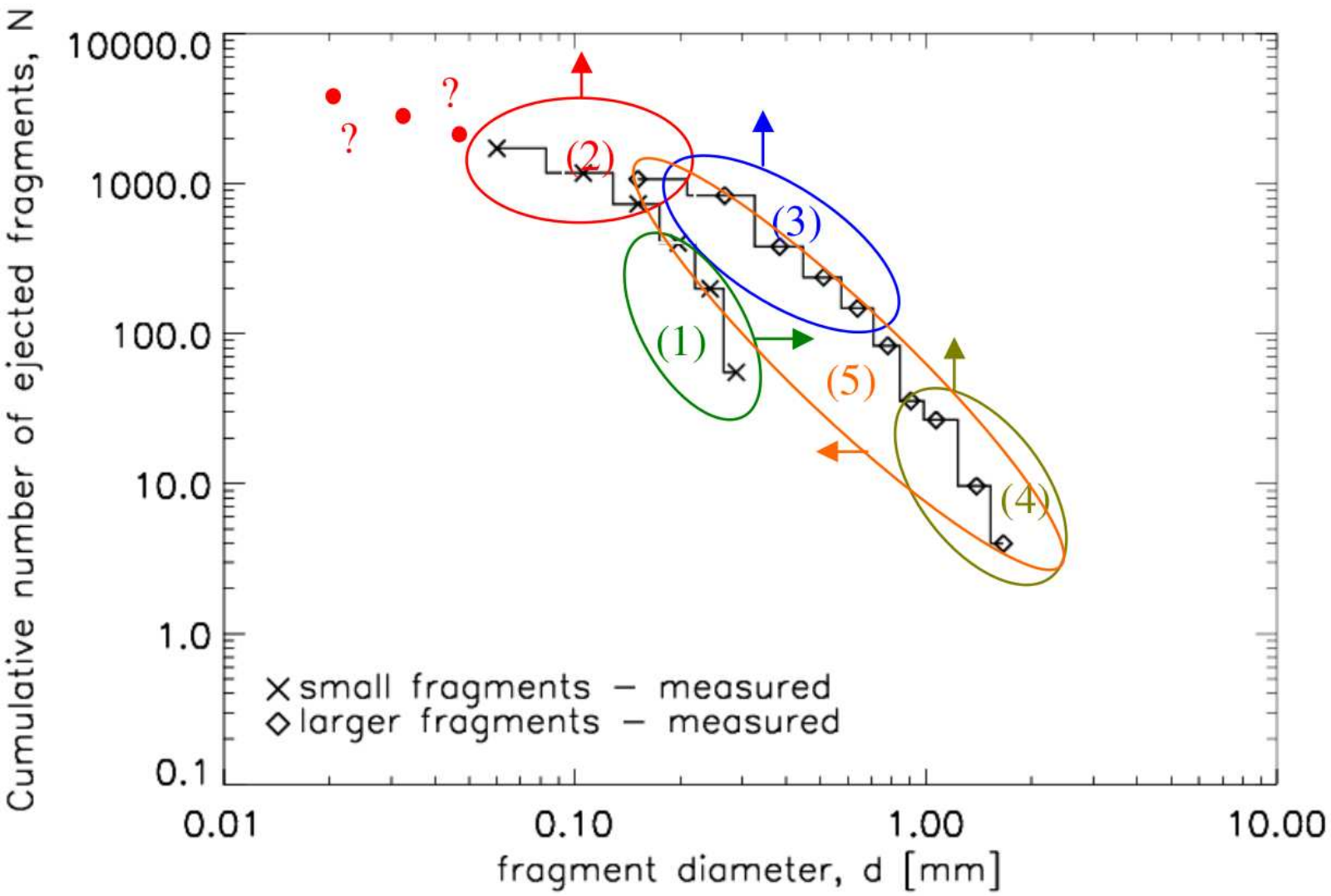

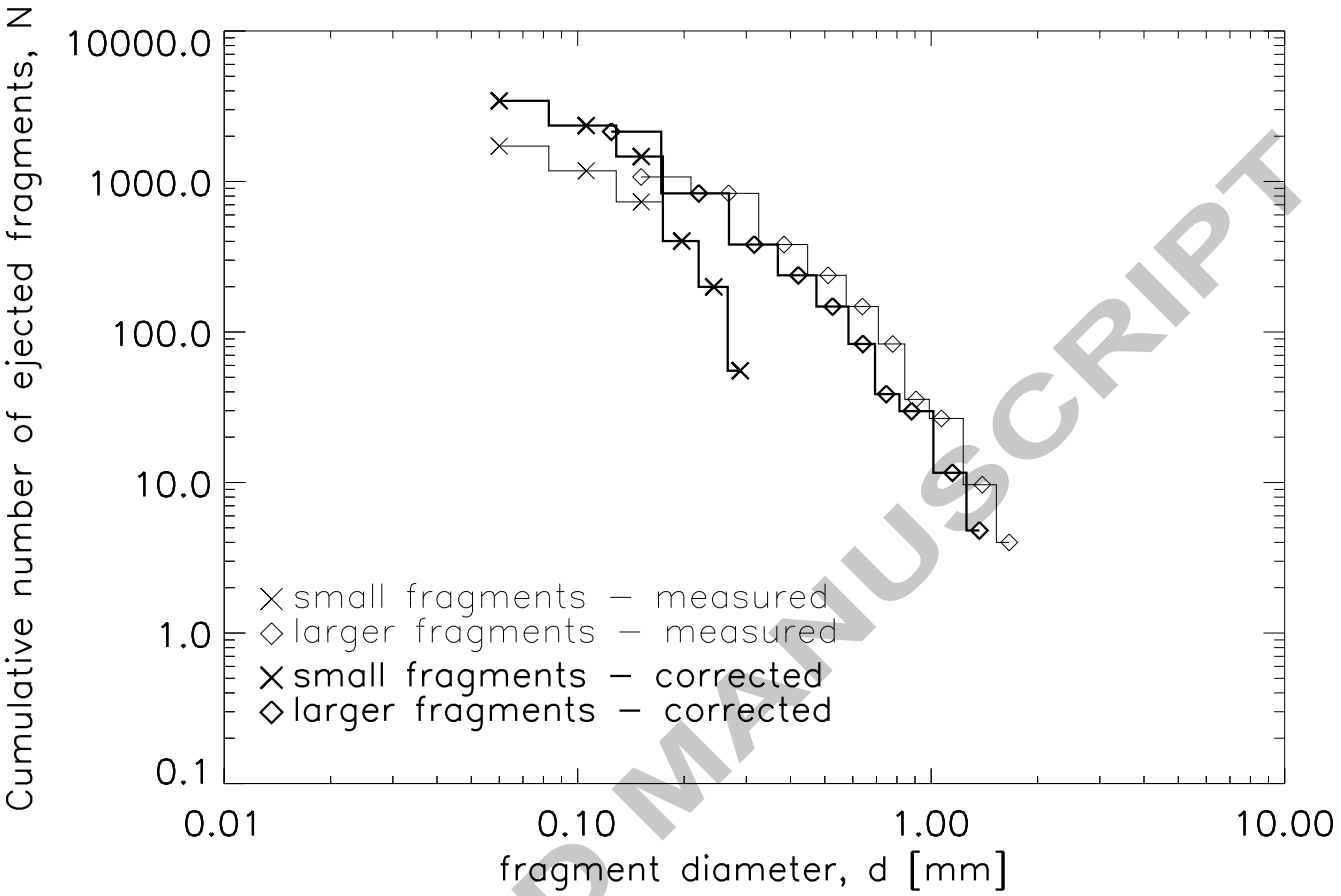

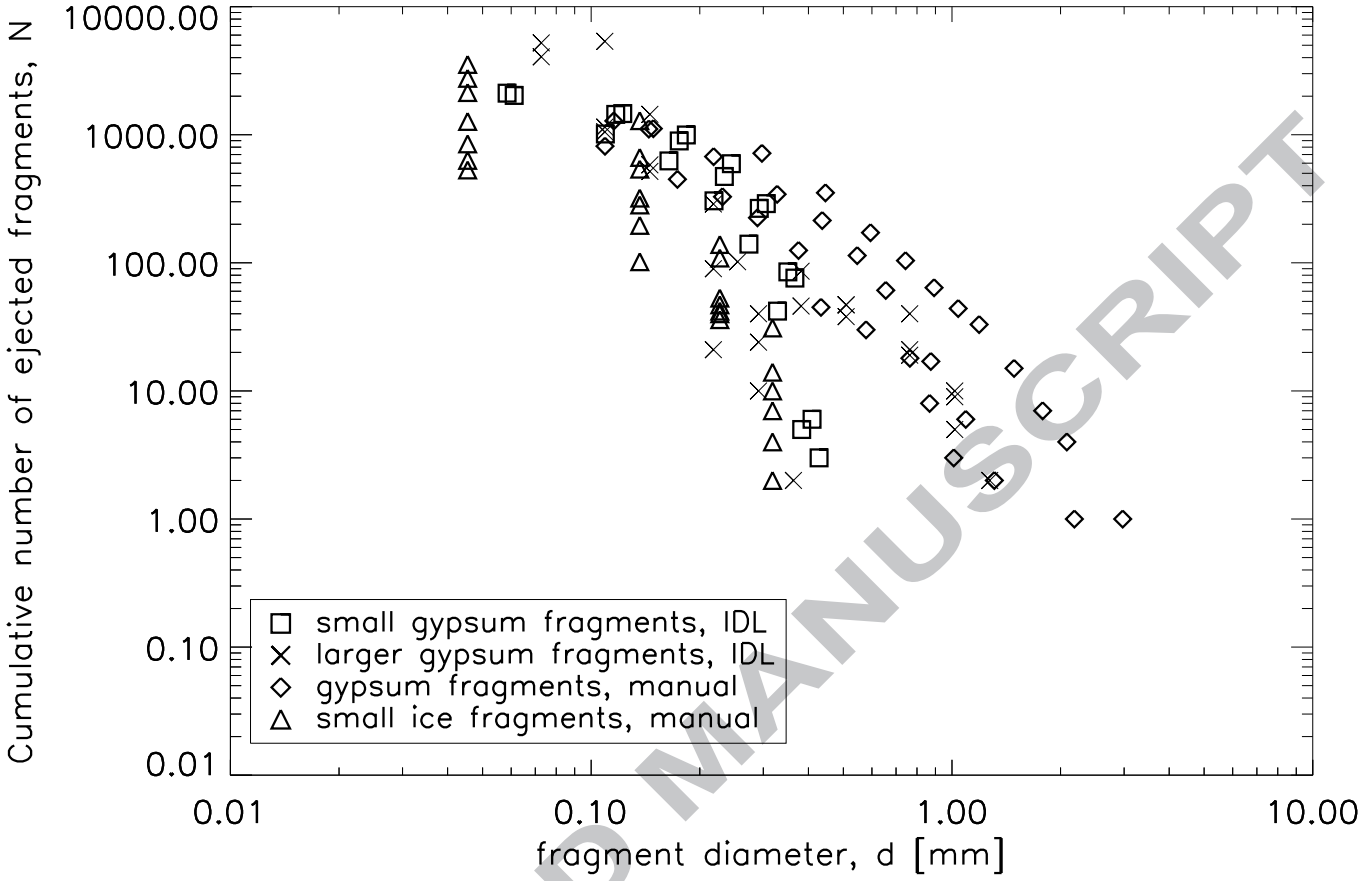

Research highlights

- The size distribution of impact induced solid ejecta from gypsum and water ice has been investigated in impact experiments.
- Preliminary results show that the size distribution of the ejecta fragments from water ice is very similar to those from gypsum.
- The comparison with other authors for similar materials at a range of impact conditions indicated that the fragmentation seems not to be strongly dependent on impact parameters such are projectile material, size, velocity, or incident angle.
- These results represent a step towards a better understanding of ejecta fragmentation in geological materials, which could also be used as icy planetary surface analogues.